AGU ADVANCING EARTH AND SPACE SCIENCE

Water Resources Research

RESEARCH ARTICLE
10.1029/2021WR030367

Asymmetry of Western U.S. River Basin Sensitivity to Seasonally Varying Climate Warming

Zhaoxin Ban[1] and **Dennis P. Lettenmaier**[1]

[1]Department of Geography, University of California-Los Angeles, Los Angeles, CA, USA

Key Points:

- Annual streamflow relative response to seasonal warming (asymmetry) is similar between large and HUC-8 basins across the Western U.S
- Vegetation enhances, while long-term snowpack-decline reduces, the asymmetry of annual streamflow response to seasonal warming
- Vapor pressure deficit and surface resistance dominate asymmetry aside from a few of the coldest basins where radiation controls

Supporting Information:

Supporting Information may be found in the online version of this article.

Correspondence to:

D. P. Lettenmaier,
dlettenm@ucla.edu

Citation:

Ban, Z., & Lettenmaier, D. P. (2022). Asymmetry of Western U.S. river basin sensitivity to seasonally varying climate warming. *Water Resources Research*, *58*, e2021WR030367. https://doi.org/10.1029/2021WR030367

Received 10 MAY 2021
Accepted 6 FEB 2022

Author Contributions:

Conceptualization: Zhaoxin Ban, Dennis P. Lettenmaier
Data curation: Zhaoxin Ban, Dennis P. Lettenmaier
Formal analysis: Zhaoxin Ban, Dennis P. Lettenmaier
Funding acquisition: Dennis P. Lettenmaier
Investigation: Zhaoxin Ban
Methodology: Zhaoxin Ban, Dennis P. Lettenmaier
Project Administration: Dennis P. Lettenmaier
Resources: Zhaoxin Ban, Dennis P. Lettenmaier
Software: Zhaoxin Ban
Supervision: Dennis P. Lettenmaier
Validation: Zhaoxin Ban, Dennis P. Lettenmaier

Abstract Future climate warming over the Western U.S. (WUS) is projected to be greater in summer than winter. Previous model-based studies of large river basins in the WUS showed much different annual streamflow responses to warming in warm versus cool seasons. However, it remains unclear how the annual streamflow relative responses to seasonal warming (asymmetry) and drivers of the response asymmetry vary across the entire WUS at the catchment-scale, and how the simulated results compare with observations. Here, we investigate the asymmetry of annual streamflow responses to warm versus cool season warming at the HUC-8 level across the entire WUS using model simulations and observations. We also examine the asymmetries' relationship with land surface and hydroclimate characteristics, and the primary contributor to the response asymmetry for each HUC-8 basin. The HUC-8 level results reveal more complexity than do earlier analyses of much larger river basins. Over 25% of WUS area has annual streamflow increases in response to warming in at least one season (mostly cool season). Annual streamflow is most sensitive to warm season warming in cool, inland basins, especially the northern Columbia River basin and most of the Upper Colorado River Basin, and most sensitive to cool season warming in warm, coastal basins. This bi-directional pattern is enhanced by vegetation coverage but weakened by long-term snowpack decline. In coldest basins with short snow-free seasons, net radiation changes dominate the streamflow response asymmetry. For basins with cold-to-intermediate temperatures, vapor pressure deficit changes dominate. For warmest basins, surface resistance changes dominate.

1. Introduction

More than 26% of the global land area and ~8% of the global population depend on snowmelt as their dominant water resource (Qin et al., 2020). Water availability in snowmelt-dominated regions may change as snow accumulations decline under climate warming, threatening the regions' economic, social, and ecological water uses (Adam et al., 2009; Barnett et al., 2005).

The winter accumulation and spring melting of snow play a major role in the seasonal water supply for the Western U.S. (WUS), which is typical of many snow-dominated regions globally. Over the past decades, warming in the WUS has caused notable changes in the seasonal timing of runoff (Stewart et al., 2004), the fraction of runoff attributable to snowmelt (Qin et al., 2020), and annual runoff decreases (Forbes et al., 2018; Milly & Dunne, 2020). Warming in the WUS is not evenly distributed on a sub-annual scale, with substantially larger warming in the warm season (Apr–Sep) than in the cool season (Oct–Mar) projected across most of the region (Ban et al., 2020; Das et al., 2011; Rupp et al., 2017). Different seasons' warming in the snowmelt dominated basins of the WUS will alter streamflow volumes quite differently. Cool season warming causes slower snow accumulation and earlier snowmelt, which may exacerbate dry-season water scarcity due to reduced storable snowmelt (Li et al., 2017). Warm season warming may cause larger peak flows that will strain reservoir capacities and may cause larger evaporative losses in summer (Li et al., 2017). Both season's warming may contribute to water scarcity, but their relative impact can substantially differ due to different seasonal warming magnitudes and seasonal sensitivities to warming (Ban et al., 2020; Vano et al., 2015). To better predict streamflow responses to climate warming and adapt to future water scarcity, understanding the streamflow sensitivity to seasonally varying climate warming is essential.

Only a few studies have examined the relative impact of differential seasonal warming on the streamflow sensitivity of WUS basins. Das et al. (2011) used the Variable Infiltration Capacity model (VIC; Liang et al., 1994) to simulate streamflow responses to seasonal warming for four regionally important river basins in the WUS. Vano and Lettenmaier (2014) and Vano et al. (2015) quantified the streamflow sensitivity to seasonal warming in

Visualization: Zhaoxin Ban
Writing – original draft: Zhaoxin Ban
Writing – review & editing: Zhaoxin Ban, Dennis P. Lettenmaier

the Colorado River basin (at basin-scale), and the Pacific Northwest (HUC-8 level). Notwithstanding this work and seasonal differences in projected future warming (Ban et al., 2020; Das et al., 2011; Hayhoe et al., 2004), questions remain as to the impacts of seasonally differential warming. These include the signature of streamflow responses to seasonal warming, which season's warming most strongly affects annual streamflow volumes, and the processes that dominate asymmetrical streamflow responses to seasonal warming. The answers to these questions have implications for the societal response to changing streamflow, especially in the water short WUS. To date, aside from Vano et al. (2015) (HUC-8 level over the Pacific Northwest) most studies that have addressed seasonal warming signatures on streamflow have been at the scale of large continental rivers (Ban et al., 2020; Das et al., 2011).

Our previous work (Ban et al., 2020) studied streamflow responses to seasonal warming for four regionally important river basins in the WUS using four hydrological models. It defined streamflow response asymmetry (termed Pref_Q as explained in Section 3.2) as the ratio of annual streamflow decreases under warm season warming to annual streamflow decreases for the same temperature increment in the cool season. Using this definition, Ban et al. (2020) concluded that river basins with two features have larger annual streamflow decreases for warm season warming as contrasted with cool season warming. The first feature is relatively cool temperature. The other is a relatively large ratio of warm season to cool season Gross Incoming Water (GIW), defined as initial water storage in soil and snow in the season plus the season's precipitation (Ban et al., 2020). However, their analysis was based on relatively large basins (15,000–600,000 km^2 drainage areas), which suppresses spatial variability that might be apparent for smaller river basins. Moreover, the ability to explore the impact of other basin surface characteristics (apart from temperature and water availability) on the streamflow responses, and how the model simulations compared with observation-based streamflow responses was limited by the large size, and small number of the basins analyzed in that study.

Here, we expand the study area to the entire WUS at the HUC-8 level. We also explore observation-based annual streamflow sensitivities in comparison with model-based estimates, and evaluate the relative role of net radiation as drivers of annual streamflow sensitivity to seasonal warming under different potential evapotranspiration frameworks (Priestley–Taylor and Penman–Monteith). Our aim in enlarging the number of basins relative to Ban et al. (2020) goes beyond simply extending our earlier analysis. Rather, the higher granularity (HUC-8) allows us to explore issues that Ban et al. (2020) and Das et al. (2011) were unable to test or explain, including statistically meaningful evaluation of similarity between simulated and observational streamflow response signals, and how those responses vary with basin characteristics and hydroclimatic factors. We also go beyond our earlier work in providing a new proxy for directly calculating the main contributor to the asymmetry of annual streamflow responses to warm and cool season warming (hereafter streamflow response asymmetry). Motivated by these goals, we address here three questions:

1. How does the annual streamflow response asymmetry vary spatially across the WUS at the HUC-8 scale, and what controls the associated spatial patterns?
2. How does the streamflow response asymmetry at HUC-8 scale vary with different land surface characteristics, such as vegetation coverage, root depth, runoff ratio, and seasonal snow coverage?
3. What are the primary contributors to annual streamflow response asymmetry for each HUC-8 basin, and do they vary across the WUS?

To address these questions, we first examine the annual streamflow responses to seasonal warming across the 616 HUC-8 basins that comprise the WUS using VIC model simulations (Section 4.1) and compare the simulated sensitivities with those estimated from observations (Section 4.2). We then examine the variation of annual streamflow responses to seasonal warming with different hydroclimatic and land surface characteristics (Sections 4.3 and 4.4). Finally, we attribute and quantify the contribution of different ET-related processes, such as warming-induced changes in net radiation, vapor pressure deficit, and surface resistance to streamflow response asymmetry across the 616 HUC-8 basins (Section 4.5). We discuss the results in Section 5 in light of a comparison between the streamflow response attribution using the Penman–Monteith framework as contrasted with the Priestley–Taylor framework in Milly and Dunne (2020), and end with conclusions in Section 6.

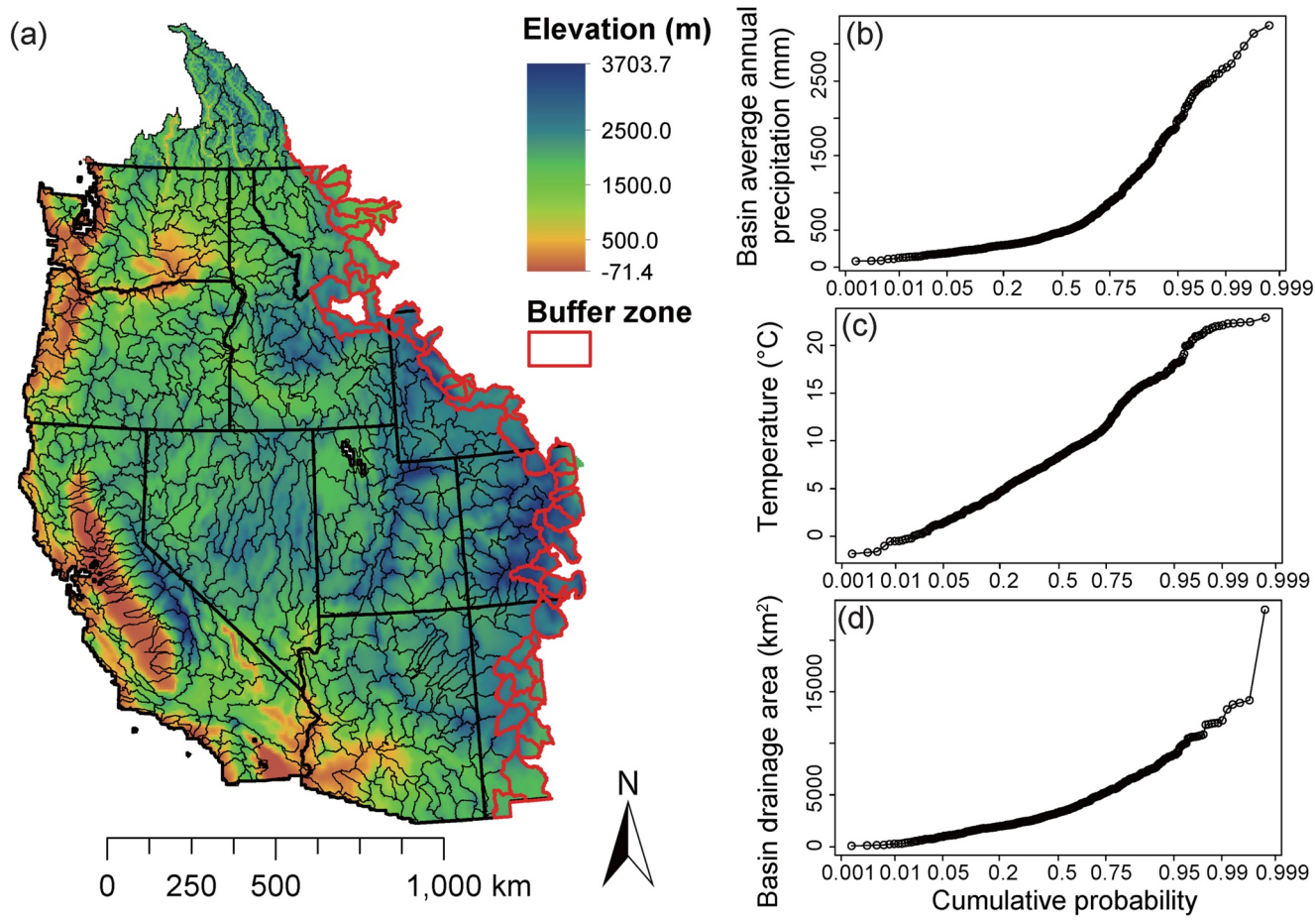

Figure 1. 616 HUC-8 basins in our study area, which covers the WUS, the Canadian portion of the Columbia River Basin, and a set of buffer basins (red outlines) just east of the Continental Divide. (a) Elevation (Gesch et al., 1999). (b) and (c) Cumulative distribution functions (CDF) of long-term climatological basin-average annual precipitation (mm) and annual mean temperature (°C), averaged from water year 1951 to 2018 using the Livneh (L13) meteorological forcings (Livneh et al., 2013), and forcings extended to 2018 by Su et al. (2021). (d) CDF of basin drainage areas.

2. Study Area

Our study domain consists of the WUS and the Canadian part of the Columbia River Basin. Additionally, we added a buffer of one HUC-8 basin width east of the Continental Divide to examine whether this geographical divide also separates the characteristics of streamflow response to seasonal warming. The study area covers a wide range of hydroclimatic conditions and land surface characteristics, with elevations ranging from below sea level (−71 m) to around 3,700 m (Figure 1a). A total of 616 HUC-8 basins are included in the study area, with an average drainage area of about 4,000 km^2. We took HUC-8 basin boundaries from the USGS National Hydrography Data set (Simley & Carswell, 2009).

3. Methods and Data

3.1. Model and Forcing Data Set

We conducted warming experiments using the VIC macroscale land-surface hydrology model (Liang et al., 1994) version (4.1.2). The VIC model forcings and parameters are the same as in Ban et al. (2020). The analysis period differs, though, with water years 1915–1950 used for spin up and water years 1951–2018 used for analysis. We chose the VIC model for our simulations because the VIC model results were closest to the multi-model mean simulated streamflow sensitivities to warming from four land surface models in Ban et al. (2020), and to observed

hydrographs relative to the other models in our previous work (Ban et al., 2020). The new analysis period was selected to check the robustness of the conclusions in Ban et al. (2020) for different simulation periods and because the forcing data quality is generally higher after 1950.

3.2. Annual Streamflow Response Asymmetry Under Seasonal Warming

We first calculated the temperature sensitivity of annual streamflow and evapotranspiration to warm and cool season warming by comparing the baseline simulation with two seasonal warming simulations. We conducted the baseline simulation using historical L13 forcings, extended to 2018 by Su et al. (2021). We set up the two seasonal warming simulations by adding 1°C to both daily maximum and minimum temperatures in every day of (a) the warm season only, and (b) the cool season only. Perturbing both maximum and minimum temperature ensures that the downward shortwave radiation generated by the Mountain Microclimate Simulation Model (MTCLIM) embedded in VIC (Bohn et al., 2013) is not changed. Downward and emitted longwave radiation from MTCLIM do change, as they are temperature-related. We isolated the warming impact on temperature sensitivity by keeping the precipitation unperturbed.

We calculated the temperature sensitivities of annual streamflow, annual evapotranspiration, and seasonal evapotranspiration as changes of their long-term averages (from water years 1951 to 2018) between a baseline and warmed scenarios, divided by the temperature increment (1°C). In all cases, temperature sensitivities are reported for each of the 616 HUC-8 basins. For pixels that are partially within a river basin, we counted the grid cell's values weighted by their fractional area in the basin.

We applied the same measure of response asymmetry to describe the relative responses of annual streamflow ($\mathrm{Pref_Q}$) and evapotranspiration ($\mathrm{Pref_{ET}}$) to seasonal warming, as was used in Ban et al. (2020) (Equations 1 and 2).

$$\mathrm{Pref_Q} = \frac{\overline{Q_{\mathrm{a,w1d}}} - \overline{Q_{\mathrm{a,b}}}}{\overline{Q_{\mathrm{a,c1d}}} - \overline{Q_{\mathrm{a,b}}}} \tag{1}$$

$$\mathrm{Pref_{ET}} = \frac{\overline{\mathrm{ET_{a,w1d}}} - \overline{\mathrm{ET_{a,b}}}}{\overline{\mathrm{ET_{a,c1d}}} - \overline{\mathrm{ET_{a,b}}}} \tag{2}$$

On the right-hand side of Equations 1 and 2, Q indicates streamflow, ET indicates evapotranspiration, the first subscript indicates the period of calculation (a: annual, w: warm season, and c: cool season), and the second subscript indicates the warming scenario (w1d: warm season 1°C warming, c1d: cool season 1°C warming, and b: baseline). Therefore, $\mathrm{Pref_Q}$ ($\mathrm{Pref_{ET}}$) is defined as the ratio of annual streamflow (annual evapotranspiration) changes in response to a constant warming magnitude (1°C) in warm season only to the same change in cool season only. A more positive $\mathrm{Pref_{ET}}$ ($\mathrm{Pref_Q}$) indicates a stronger "preference" for a basin to have stronger annual evapotranspiration (streamflow) response under warm versus cool season warming. A negative $\mathrm{Pref_{ET}}$ ($\mathrm{Pref_Q}$) means that the annual evapotranspiration (streamflow) responses have opposite signs under the two seasonal warming. According to the long-term water balance, when the annual soil and snow storage change is negligible and precipitation is fixed, the annual streamflow reduction under temperature warming equals the annual evapotranspiration increase. Under this water balance framework, Ban et al. (2020) made two critical assumptions: (a) $\mathrm{Pref_Q} \approx \mathrm{Pref_{ET}}$, and (b) the relative rank of $\mathrm{Pref_{ET}}$ across basins is governed by the relative rank of the seasonal ET-T sensitivity ratios (ratios of warm season ET-T sensitivity to cool season ET-T sensitivity, see Equation 3, the notation is the same as in Equations 1 and 2).

$$\mathrm{rank}(\mathrm{Pref_{ET}}) = \mathrm{rank}\left(\frac{\overline{\mathrm{ET_{w,w1d}}} - \overline{\mathrm{ET_{w,b}}}}{\overline{\mathrm{ET_{c,c1d}}} - \overline{\mathrm{ET_{c,b}}}}\right) \tag{3}$$

Ban et al. (2020) tested the above two assumptions for four major river basins in the WUS (the Columbia, the Upper Colorado River basin (hereafter UCRB), and the Northern Sierra and Southern Sierra basins). Here, we tested the two assumptions by comparing the $\mathrm{Pref_{ET}}$, $\mathrm{Pref_Q}$, and seasonal ET-T sensitivity ratios across all 616 HUC-8 basins.

3.3. Annual Streamflow Response Asymmetry Estimated From Observations

We checked whether our model-based streamflow response asymmetry could be reproduced using observations of annual streamflow from two sources: (a) USGS GAGES Version 2 (GAGES II) reference database, which are

identified as stations with minimum anthropogenic disturbances (Falcone, 2011), and (b) USGS WaterWatch streamflow data (Brakebill et al., 2011), which provides a relatively complete set of streamflow data at the HUC-8 level from water year 1951 to 2018. In the GAGESII database, we only chose the gages with more than 20 years that have more than ~11 months (335 days) record each year, resulting in 513 GAGESII stations. We also performed a screening of the WaterWatch records to remove the HUC-8 basins with USGS stations affected by large dams. Specifically, we identified large dams as having storage capacity greater than a quarter of the long-term average annual streamflow based on data from the Global Reservoir and Dam Database (GranD v1.3; Lehner et al., 2011). This screening yielded 286 HUC-8 basins as having annual flows that are at most modestly affected by reservoir regulations.

For each selected GAGESII station's contributing area and each screened WaterWatch HUC-8 basin, we calculated the corresponding annual precipitation (P_a) and seasonal mean temperature (T_w and T_c) from VIC model outputs. We applied linear regression at each of the 513 GAGESII stations across years with more than 11 months record, and 286 screened WaterWatch HUC-8 basins across water year 1951 to 2018 using annual streamflow (Q_a) as the dependent variable, and P_a, T_w, and T_c as predictors (Equation 4).

$$Q_a = S_w T_w + S_c T_c + S_p P_a \tag{4}$$

In Equation 4, S_w, S_c, and S_p are the regression coefficients. Pref_Q thus is estimated as S_w/S_c. In Section 4.2, we focus more on the Pref_Q estimates for basins that have both statistically significant ($p = 0.1$) S_w and S_c.

3.4. Relationships Between Annual Streamflow Response Asymmetry and Basin Characteristics

We checked the variations of seasonal ET-T sensitivity (a proxy governing streamflow response asymmetry, tested in Sections 3.2 and 4.1) with temperature and seasonal water availability at the HUC-8 basin level. We used simulated basin-average temperature and GIW, and basin-aggregated seasonal evapotranspiration across the 616 HUC-8 basins from the VIC control experiment outputs to carry out the check. In addition to the above two hydroclimate variables, we also incorporated seven basin land surface and hydroclimatic characteristics:

1. Elevation: 1/16th degree, aggregated from the GTOPO30 Global 30 Arc Second (~1 km) Elevation Data set (Gesch et al., 1999)
2. Runoff ratio, snow cover fraction, and annual mean snow water equivalent (SWE): VIC baseline simulation outputs in this paper
3. Vegetation density: product of the annual mean leaf area index (LAI) and the vegetation cover fraction for each vegetation type summed for each pixel, where LAI and vegetation cover fraction came from the VIC vegetation parameter file
4. Root depth: sum of root depth for each vegetation type weighted by the vegetation cover fraction for each pixel, where the root depth and vegetation cover fraction came from the VIC vegetation parameter file
5. Vegetation height: sum of vegetation height for each vegetation type weighted by the vegetation cover fraction for each pixel, where the vegetation height and vegetation cover fraction came from the NLDAS vegetation classification scheme (Hansen et al., 2000) and parameters (https://ldas.gsfc.nasa.gov/nldas/vegetation-parameters)

We classified the 616 HUC-8 basins based on the seven characteristics and examined how the asymmetries of seasonal ET-T sensitivity and annual streamflow response to seasonal warming vary with the seven characteristics above.

3.5. Detection of the Processes Dominating ET-T Sensitivity

We considered five major processes that affect evapotranspiration change under temperature warming, as derived using a Penman–Monteith framework (e.g., Ban et al. (2020) and Yang et al. (2019)): (a) change of available radiation (R*, net radiation minus ground heat flux) due to processes like albedo change during snowmelt, (b) enhanced vapor–pressure deficit (e_s-e_a) associated with warming, (c) increased surface resistance (r_s) associated with elevated vapor pressure deficit, (d) reduced aerodynamic resistance (r_a) over warmer, less stable land surfaces, and (e) elevated slope of the saturated vapor pressure δ associated with warming. We estimated

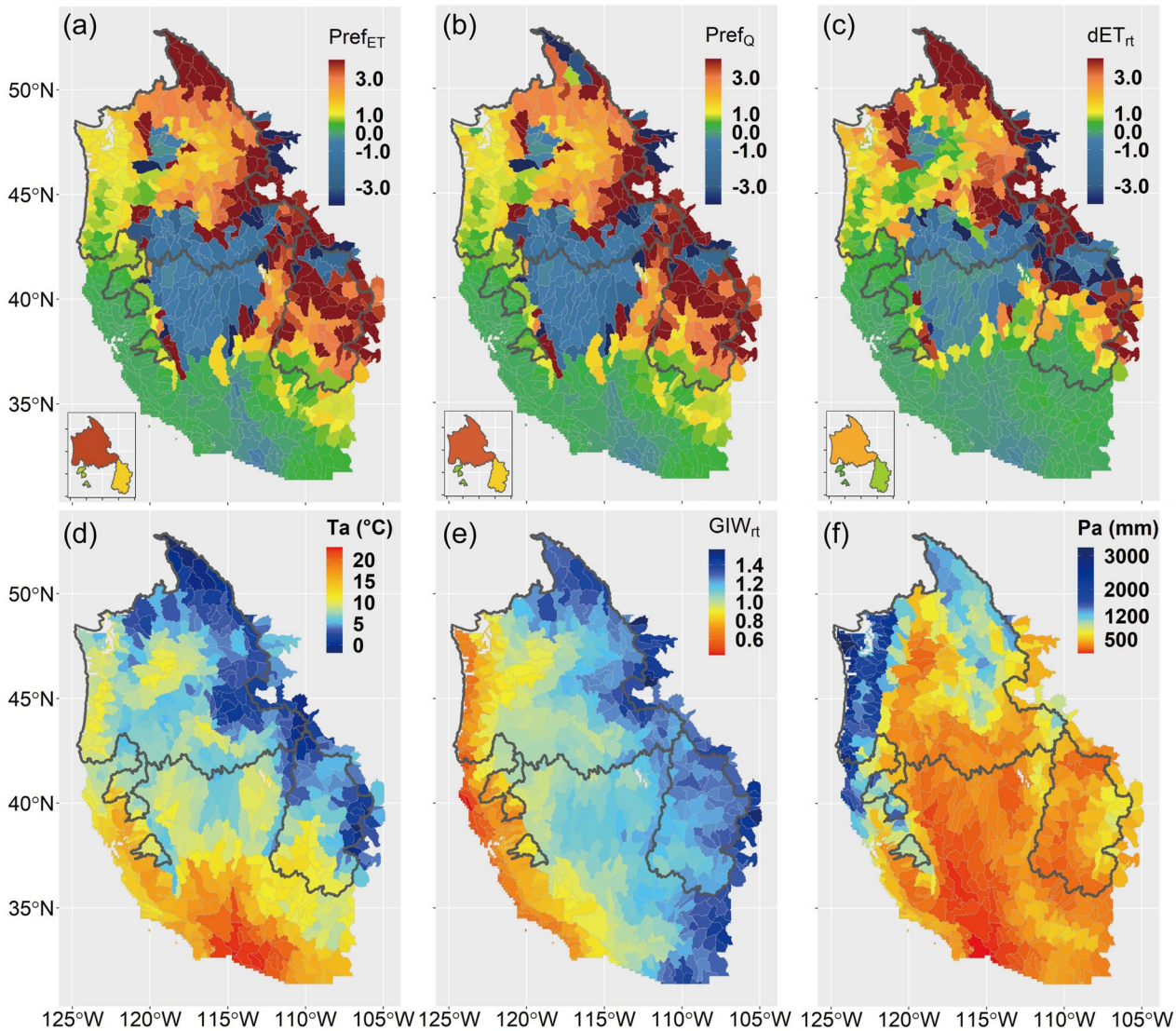

Figure 2. Proxies of response asymmetry and related variables. (a) $Pref_Q$, (b) $Pref_{ET}$, and (c) seasonal ET-T sensitivity ratio (dET_{rt}) under 1°C warm and cool season warming from the VIC-4.1.2 model results for HUC-8 basins, averaged from the water year 1951 to 2018. The small panels illustrate the basin-average values from multi-model mean results in Ban et al. (2020). (d) Basin average annual mean temperature, (e) GIW_{rt}: ratio of basin average warm season Gross Incoming Water (GIW) to basin average cool season GIW, (f) basin average annual precipitation. All values in (d) to (f) are based on climatologies from water year 1951 to 2018.

contributions of the five processes to seasonal ET-T sensitivity using a Penman–Monteith first-order derivative expansion based on differences between the two season's warming scenarios and baseline, which is the same as in Section 3.6 in Ban et al. (2020).

4. Results

4.1. Asymmetry of Annual Streamflow Responses to Seasonal Warming

To check the similarity between the seasonal ET-T sensitivity ratio (see Equation 3), $Pref_Q$, and $Pref_{ET}$ (see Equations 1 and 2), we plotted their spatial distributions (model-simulated) at the HUC-8 level (Figures 2a–2c). The three proxies show highly consistent spatial patterns, as indicated by their pattern correlation values: $Pref_{ET}$ versus $Pref_Q$: 0.995, $Pref_Q$ versus dET_{rt}: 0.796, $Pref_{ET}$ versus dET_{rt}: 0.795 (we calculated pattern correlations using samples within 5% and 95% percentile of the proxies to remove outliers). The consistent spatial patterns are similar to those in Ban et al. (2020) for larger basins (smaller panels in Figures 2a–2c, values in those smaller panels are consistent with the cumulative effect expected from the HUC-8 basins involved). Additionally, proxies

for HUC-8 basins east of the Continental Divide act mostly like neighbors west of the divide, suggesting strong spatial continuity.

In general, among basins with positive Pref (hereafter referring to both $Pref_Q$ and $Pref_{ET}$) values, basins with larger responses to warm season warming (higher Pref values) are located within the northeast part of the study domain. Basins with smaller responses to warm season warming (lower Pref values) are located within the southwestern part of the study domain (Figures 2a–2c). This southwest-northeast gradient in Pref values generally coincides with the direction of decreasing annual temperature and increasing warm versus cool season GIW ratio (Figures 2d and 2e), which follows the conclusion in Ban et al. (2020).

The HUC-8 level maps of the three proxies (Figures 2a–2c) however reveal more complexity than do the larger basin maps, especially concerning negative Pref values. In Ban et al. (2020), multi-model mean Pref values for all four basins were positive, but at the HUC-8 level, negative Pref values are present for some basins and usually are clustered. Negative $Pref_{ET}$ or $Pref_Q$ values are caused by annual evapotranspiration decrease or annual streamflow increase only under one of the two seasonal warming cases (mostly under cool season warming). No basin has annual evapotranspiration (streamflow) decreases (increases) under both warming scenarios. Therefore, the positive $Pref_{ET}$ and $Pref_Q$ values are only related to the annual evapotranspiration (streamflow) increase (decrease) under both warming scenarios. The Columbia Basin has the largest area with negative Pref values, which cluster in the southern part of the basin (mostly arid to semi-arid, and borders on the Great Basin). The UCRB has negative Pref values in the northeastern part, while the two California basins have no negative Pref values. To further explore the relationship between seasonal responses and the sign and magnitude of Pref, we classified the basins into snow-affected (basin long-term mean Apr 1st SWE $\geq$20 mm) and non-snow-affected group (basin long-term mean Apr 1st SWE <20 mm). We divided each group into four subgroups according to different signs and magnitudes of Pref values (Figure 3):

A. *Snow-affected (SA) group.* 301 of 616 basins (48.86%; the colored basins in the first row of Figure 3).

A1. *Pref positive and larger than 1.0*, colored in red in Figures 3a–3b. In such basins, annual evapotranspiration (streamflow) increases (decreases) are stronger under warm season warming than under cool season warming. 218 of the 301 snow-affected basins for $Pref_{ET}$ (72.4%) and 209 of 301 snow-affected basins for $Pref_Q$ (69.4%) had these characteristics. Most of them coincide with ET-T sensitivity ratios that are positive and larger than 1.0 (colored red in Figure 3c).

A2. *Pref positive and smaller than 1.0*, colored in brown in Figures 3a–3b. In such basins, annual evapotranspiration (streamflow) increases (decreases) are stronger under cool season warming than under warm season warming. The 61 of 301 snow-affected basins for $Pref_{ET}$ (20.3%) and 67 of 301 snow-affected basins for $Pref_Q$ (22.3%) had these characteristics. Most of them coincide with ET-T sensitivity ratios that are positive and smaller than 1.0 (colored brown in Figure 3c).

A3. *Pref negative and smaller than −1.0*, colored in dark blue in Figures 3a–3b. The 19 of 301 snow-affected basins for $Pref_{ET}$ (6.3%), and 22 of 301 snow-affected basins for $Pref_Q$ (7.3%) had these characteristics. Most of them coincide with the ET-T sensitivity ratios that are more negative than −1.0 (colored dark blue in Figure 3c). The 19 negative $Pref_{ET}$ values are all caused by annual evapotranspiration decreases under cool season warming. Among these 19 basins, responses for 10 basins are contributed solely by cool season evapotranspiration decreases, responses for five basins are contributed solely by warm season evapotranspiration decrease, and responses for four basins are contributed by both warm and cool season evapotranspiration decreases (Figure S2a in Supporting Information S1). Among the 22 negative $Pref_Q$ values, 19 are caused by cool season streamflow increases under cool season warming, and three are caused by warm season streamflow increases under warm season warming (Figure S2b in Supporting Information S1). The latter three basins are in the northern part of the Columbia basin, at high elevation with short snow-free seasons and relatively lower vegetation density and shallower root depths than the surroundings (Figure S1 in Supporting Information S1). They have much later snowmelt season end dates than low elevation basins and have streamflow increases only in the warm season. The annual streamflow increase magnitudes in these three basins are relatively small (all less than 1%). These three basins do not have annual evapotranspiration decreases, suggesting that the slight annual streamflow increases at these three high elevation basins are associated with snowpack declines.

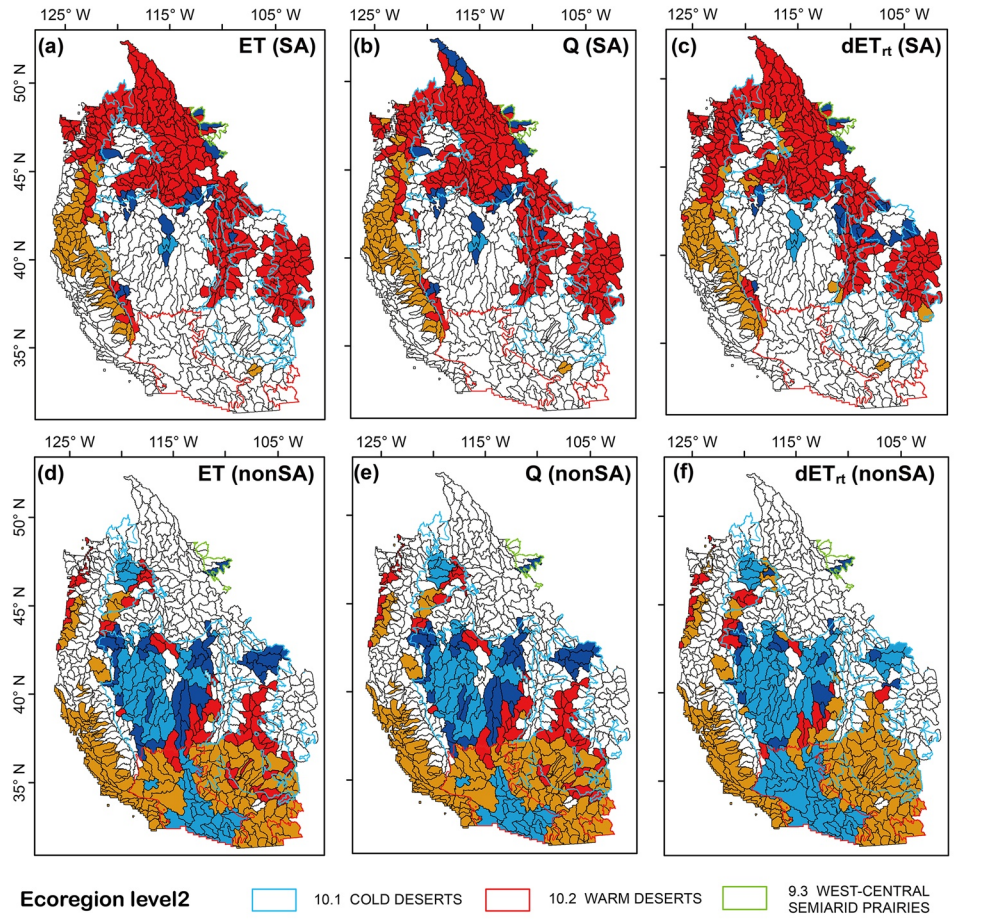

Prefs and dET$_{rt}$	SA (301 basins)	nonSA (315 basins)
More than 1	A1: Inland, high latitude/elevation basins ~71% of SA.	B1: Inland, high latitude/elevation basins ~19% of nonSA.
(0,1)	A2: Coastal moist basins ~21% of SA.	B2: Coastal moist, or low-latitude, moderate warm basins. ~49% of nonSA.
Less than -1	A3: Cool and arid, or extremely cold, long snow season basins. ~7% of SA.	B3: Cool and arid basins. ~11% of nonSA.
[-1,0)	A4: Cool and arid basins. ~1% of SA.	B4: Cool and arid, or warm desert basins. ~21% of nonSA.

*Prefs and dET$_{rt}$: More than 1: warm season warming dominates, (0,1): cool season warming dominates, Negative: opposite changes under two seasonal warming.

Figure 3. Map of 616 HUC-8 basins categorized based on snow-affected (SA: mean Apr 1st SWE >20 mm) or non-snow affected (nonSA: mean Apr 1st SWE <20 mm) conditions; signs of Pref$_{ET}$, Pref$_{Q}$, and ET-T sensitivity ratios (dET$_{rt}$), and their absolute values relative to 1.0 for the three indices (shown separately in subplots a-f).

A4. *Pref negative and larger than −1.0*, colored light blue in Figures 3a–3b. Three of 301 snow-affected basins (1.0%) for both Pref$_{ET}$ and Pref$_{Q}$ had these characteristics. Most of them coincide with ET-T sensitivity ratios that are less negative than −1.0 (colored light blue in Figure 3c). The negative Pref values are caused by annual evapotranspiration decreases (annual streamflow increases) under cool season warming, which have a smaller magnitude than the opposite response under warm season warming. All the three annual evapotranspiration decreases (annual streamflow increases) are solely contributed by cool season evapotranspiration decreases (streamflow increases).

For conditions A3 and A4, excepting the three high elevation basins in the northern Columbia River Basin for which annual streamflow increases under warm season warming, all other basins with negative Pref values experienced annual evapotranspiration decreases (annual streamflow increases) under cool season warming. Spatially, these latter basins are mostly located within or at the boundary of the cold desert region (Ecoregion Level-II classification: https://www.epa.gov/eco-research/ecoregions-north-america) in or near the Great Basin, and the West-Central semi-arid prairies area in the northeastern buffer zone of the Columbia River Basin boundary (Figures 3a–3b). Such regions have moderate temperatures (Figure 2d), moderate elevations (Figure S1e in Supporting Information S1), low precipitation (Figure 2f), low runoff ratios (Figure S1d in Supporting Information S1), low vegetation coverage (Figures S1a–S1b in Supporting Information S1), and low snow coverage (Figures S1f–S1g in Supporting Information S1). For these basins, the warm season evapotranspiration decreases under cool season warming can be explained by the Dettinger hypothesis (Dettinger et al., 2004): under cool season warming, earlier snowmelt releases water exiting the basin before summer comes, which leaves less water available for evapotranspiration later in the year (i.e., warm season). Possible reasons for the small decreases (all <5%) of cool season evapotranspiration under cool season warming (colored in cyan in Figure S2a in Supporting Information S1) are:

1. Those basins are mostly water-limited, thus relatively insensitive to elevated evaporative demand under warming (Condon et al., 2020)
2. Warmer cool season temperature increases the chance for cool season snowpack to melt before sublimating, which enables a larger portion of snowmelt to become streamflow or to penetrate into deeper soil layers without being sublimated (Barnhart et al., 2016), which is the dominant cool season evapotranspiration process in these basins (Table S1 in Supporting Information S1)
3. Those basins usually have thin and sparse snow coverage in the cool season. In this context, warming can cause temporally discontinuous snow coverage within the cool season, thus extending the cool season's water-limited period

B. *Non-snow-affected (nonSA) group*. 315 of the 616 basins (51.1%) were in this group (the colored basins in the second row of Figure 3).

B1. *Positive Pref greater than 1.0* (colored red in Figures 3d–3e). Annual evapotranspiration increases (annual streamflow decreases) are stronger under warm season warming than under cool season warming in these basins, of which there are 60 for $Pref_{ET}$ (19.0%), and 59 for $Pref_{Q}$ (18.7%). Most of these basins have ET-T sensitivity ratios that are positive and larger than 1.0 (colored in red in Figure 3f).

B2. *Positive Pref, less than 1.0*, colored in brown in Figures 3d–3e. Annual evapotranspiration increases (annual streamflow decreases) are stronger under cool season warming than under warm season warming for these basins, of which there are 151 for $Pref_{ET}$ (47.9%) and 154 for $Pref_{Q}$ (48.9%). Most of them have ET-T sensitivity ratios that are positive and smaller than 1.0 (colored in brown in Figure 3f).

B3. *Negative Pref, more negative than −1.0*, colored in dark blue in Figures 3d–3e. 35 basins fall into this category for $Pref_{ET}$ (11.1%) and 36 for $Pref_{Q}$ (11.4%). Most of these basins coincide with ET-T sensitivity ratios that are negative and smaller than −1.0 (colored in dark blue in Figure 3f). The negative $Pref_{ET}$ and $Pref_{Q}$ values are caused by annual evapotranspiration decreases and annual streamflow increases under cool season warming. For the 35 basins with annual evapotranspiration decreases, 25 are associated solely with cool season evapotranspiration decreases, seven are associated solely with warm season evapotranspiration decreases, and three have both cool season and warm season evapotranspiration decreases (Figure S2a in Supporting Information S1). For the 36 basins with annual streamflow increases, 26 are contributed solely by cool season streamflow increases, and 10 have both warm and cool season streamflow increases (Figure S2b in Supporting Information S1). All these basins are located within or near the boundary of cold desert areas. The decreasing warm season evapotranspiration under cool season warming is due to stronger soil moisture deficits in the beginning of the warm season following enhanced evapotranspiration during cool season warming. Possible reasons for the decreasing cool season evapotranspiration under cool season warming are the same as we discuss for A3 and A4 above.

B4. *Negative Pref, less negative than −1.0*, colored in light blue in Figures 3d and 3e. The 69 of 315 non-snow-affected basins for $Pref_{ET}$ (21.9%) and 66 $Pref_{Q}$ (21.0%) had these characteristics. Most of them coincide with ET-T sensitivity ratios that are less negative than −1.0 (colored in light blue in Figure 3f). For the 69

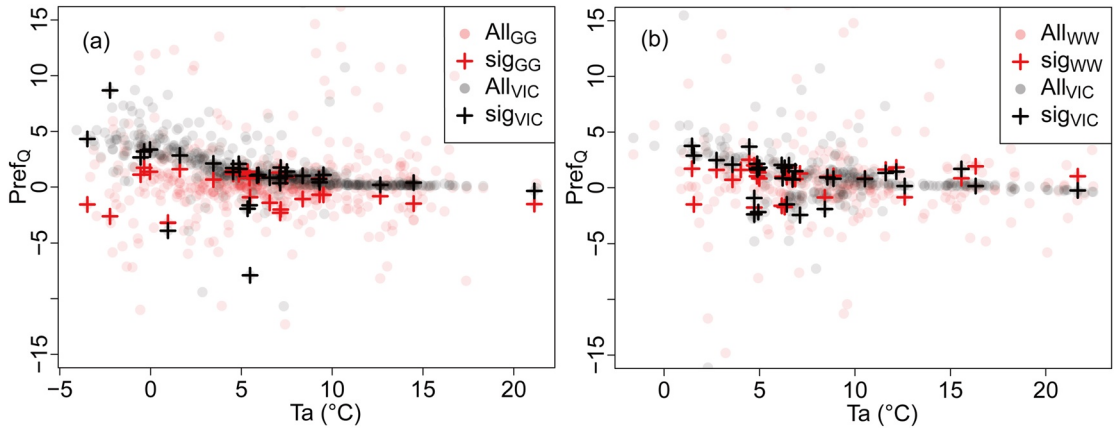

Figure 4. Point-by-point comparisons between VIC-simulated and observation-based $Pref_Q$, for (a) GAGESII (GG) basins, and (b) WaterWatch (WW) HUC-8 basins. Crosses highlight the basins that have statistically significant ($p = 0.1$) temperature regression coefficients in Equation 4, and other points show all basins' estimates.

basins that have negative $Pref_{ET}$, 27 basins are associated with warm season evapotranspiration decreases under warm season warming, 39 are associated with cool season evapotranspiration decreases under cool season warming, and three basins are associated with both warm and cool season evapotranspiration decreases under cool season warming. For the 66 basins with negative $Pref_Q$, 25 are dominated by cool season streamflow increases under warm season warming, and 41 are dominated by cool season streamflow increases under cool season warming. The 27 basins with warm season evapotranspiration decreases (which includes the 25 basins with cool season streamflow increases) under warm season warming fall into the warm desert Ecoregion Level-II classification (reddish color in Figures S2a and S2b in Supporting Information S1) near the Mojave and Sonoran Deserts. The warm desert regions generally have low precipitation (Figure 2f), low vegetation coverage (Figures S1a and S1b in Supporting Information S1), as well as low snow coverage (Figures S1f and S1g in Supporting Information S1), low runoff ratios (Figure S1d in Supporting Information S1), low elevation (Figure S1e in Supporting Information S1) and higher temperatures (Figure 2d) as compared to the cold desert type. These basins are very arid and have limited streamflow, with maximum basin average annual streamflow less than 40 mm, relative increases of annual streamflow less than 1%. The warm season evapotranspiration decreases under warm season warming in these 27 basins are mostly due to elevated surface resistance associated with warmer temperatures, which is supported by the high surface temperature part (>20°C) in Figure S3 in Supporting Information S1.

In general, the basins with negative Pref values (126 basins for $Pref_{ET}$ and 127 basins for $Pref_Q$) are in low elevation, arid regions with high temperatures and little snow coverage. These basins contribute slightly less than 9% of the total streamflow for all 616 HUC-8 basins in the WUS, according to the VIC simulation results. Although these basins have streamflow increases under certain warming scenarios, their streamflow increases tend to be small and far from enough to compensate for streamflow declines elsewhere across our WUS domain.

4.2. Observation-Based Asymmetry of Annual Streamflow Responses to Seasonal Warming

We compared all of the observation-based and VIC model-simulated $Pref_Q$ (Figures 4a and 4b) on a point-by-point basis and found that, despite differences between observation-based and simulated estimates, they share similar probability distributions, and are roughly similar in their variations with air temperature, especially the basins with statistically significant temperature regression coefficients (S_w and S_c, at $p = 0.1$ level; Figure 4 and S4 in Supporting Information S1). Comparison of Figures 4a and 4b shows that $Pref_Q$ values estimated using WaterWatch have a better match with VIC-simulated ones than do the GAGESII (USGS Reference) gauges, probably because the WaterWatch basin areas (mean drainage area 3,180 km^2) are larger than the GAGESII ones (mean drainage area 520 km^2). Both Figures 4a and 4b show decreasing $Pref_Q$ (both model- and observation-inferred) as temperature increases, despite the different spatial coverage between the two data sets (Figure S5 in Supporting Information S1). This decreasing trend echoes the pattern of lower $Pref_Q$ under warmer temperature found from multiple model simulations in Ban et al. (2020). We also conducted two similar comparisons for S_w and S_c sepa-

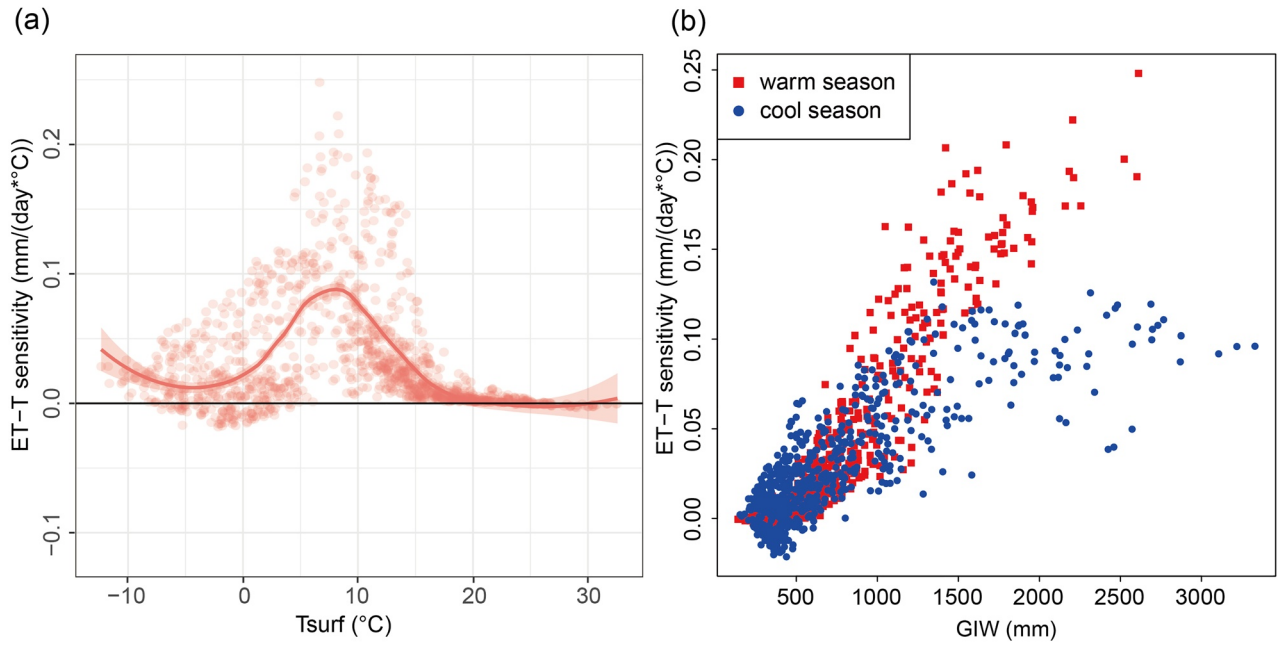

Figure 5. (a) ET-T sensitivity as a function of seasonal surface temperature (Tsurf). The red curve is LOWESS-smoothed from the seasonal values from each of the 616 HUC-8 basins. Both warm and cool season values are plotted in panel (a). The LOWESS-smooth span parameter is 0.5; shading denotes the confidence interval (level = 0.95) for the possible locations of the smoothed lines. The lower first and upper 99th percentiles of cool season temperature basins are excluded as outliers and are not plotted in this figure. (b) Relationship between ET-T sensitivity and Gross Incoming Water (GIW: initial water storage in soil and snow in the season plus the season's precipitation). Red (blue) points are for warm (cool) season. Each point denotes a basin's basin-average value.

rately (Figures S6 and S7 in Supporting Information S1), and compared $Pref_Q$ spatially (Figure S5 in Supporting Information S1), which also show some hint of similarity. The above results provide some data support to the simulated patterns and interpretations of simulated asymmetry in the following sections.

A high fraction of temperature coefficients estimated from Equation 4 are statistically insignificant (only 30 out of 513 gages, and 31 out of 286 basins are statistically significant at significance level = 0.1). Nonetheless, the significant coefficient fractions (5.8% and 10.8%) are still much larger than that can be attributed to chance (0.1*0.1 = 0.01 = 1%). Considering all the above, we argue that the similarity between model- and observation-inferred $Pref_Q$ distribution is not coincidental, which adds credibility to our model-based results.

4.3. ET-T Sensitivity as a Function of Temperature and Gross Incoming Water

In Section 4.1, we confirmed the similarity between the seasonal ET-T sensitivity ratios and the Pref values. Here, we examine another conclusion in Ban et al. (2020) relative to the variation of ET-T sensitivity with temperature and GIW (see Section 1 for definition) at the HUC-8 level. Warm and cool season ET-T sensitivities from each of the 616 HUC-8 basins are plotted together as a function of seasonal surface temperature and LOWESS-smoothed into a red curve in Figure 5a. In Figure 5b, relationships between ET-T sensitivities and GIW are plotted as scatterplots separately for warm and cool season.

The increasing-to-decreasing pattern (above −5°C) of ET-T sensitivity as temperature increases (Figure 5a) and the positive relationship between ET-T sensitivity and GIW (Figure 5b) confirm the findings in Ban et al. (2020): (a) ET-T sensitivity increases (decreases) with temperature in cool (warm) environments, so cooler basins have a higher ratio of warm to cool season ET-T sensitivity, thus higher Pref values; and (b) higher water availability favors higher ET-T sensitivity, so among basins with similar temperatures, a higher warm-to-cool-season GIW ratio favors a higher ET-T sensitivity ratio, thus higher Pref values. These relationships support the southwest-to-northeast increasing Pref values (Figures 2a–2b), west-to-east increasing GIW ratio (Figure 2e), and southwest-to-northeast decreasing annual mean temperature across the WUS (Figure 2d, which is a conse-

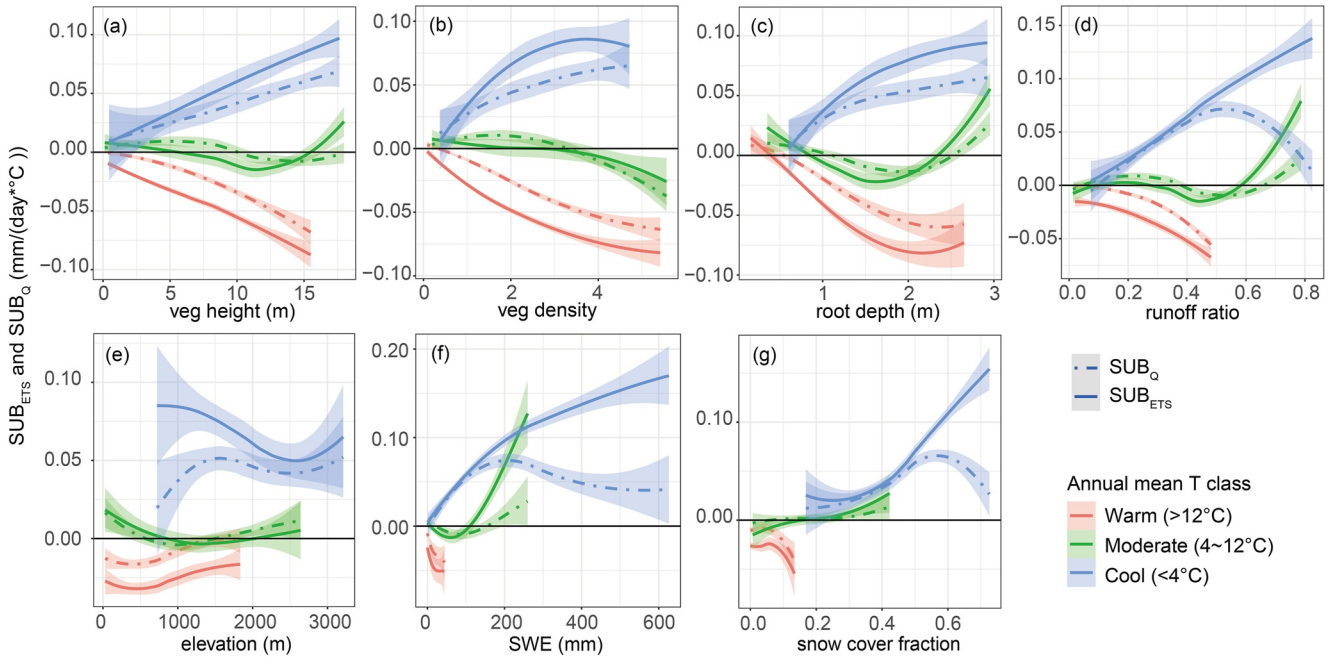

Figure 6. Variation of asymmetry of seasonal ET-T sensitivity (SUB_{ETS}), and asymmetry of annual streamflow response to seasonal warming (SUB_Q) with (a) vegetation height, (b) vegetation density, (c) root depth, (d) runoff ratio, (e) elevation, (f) climatological annual mean SWE, and (g) climatological annual mean snow cover fraction, in three different temperature zones divided according to long-term average annual mean air temperature (Cool: <4°C, Moderate: 4–12°C, and Warm: >12°C) across the HUC-8 basins. Each plot shows LOWESS-smoothed curves of scatterplots (points are not plotted for clarity) between the asymmetries and basin characteristics using values from each 616 HUC-8 basins. The LOWESS-smoothing span parameter is 1.0, shading is as in Figure 5a.

quence of the both south-to-north increasing latitude and west-to-east increasing elevation), as identified in Section 4.1. We further separated the basins into snow-affected and non-snow-affected subgroups to evaluate the patterns (Figure S8 in Supporting Information S1) and found that the patterns in Figures 5a and 5b above are generally consistent in both subgroups.

4.4. Streamflow Response Asymmetry and ET-T Sensitivity Asymmetry Across Basin Characteristics

Here we focus on the relationship among basin surface characteristics (other than temperature and water availability discussed above), the asymmetry of annual streamflow response to seasonal warming, and seasonal ET-T sensitivity asymmetry. We calculated seven basin characteristics for each of the 616 HUC-8 basins with VIC parameters and simulations (as described in Section 3.4): vegetation height, vegetation density, root depth, runoff ratio, elevation, climatological annual mean SWE, and climatological annual mean snow cover fraction (see Figures S1a–S1g for maps in Supporting Information S1). We also calculated the annual streamflow response asymmetry and ET-T sensitivity asymmetry for each of the 616 HUC-8 basins, in the form of SUB_Q and SUB_{ETS} (defined in Equations 5 and 6, notation is the same as in Equations 1–3, where Q indicates streamflow, and ETS is short for ET-T Sensitivity).

$$SUB_Q = \left(\overline{Q_{a,b}} - \overline{Q_{a,w1d}}\right) - \left(\overline{Q_{a,b}} - \overline{Q_{a,c1d}}\right) \quad (5)$$

$$SUB_{ETS} = \left(\overline{ET_{w,w1d}} - \overline{ET_{w,b}}\right) - \left(\overline{ET_{c,c1d}} - \overline{ET_{c,b}}\right) \quad (6)$$

By construct, a more positive value of SUB_Q or SUB_{ETS} means stronger annual streamflow (evapotranspiration) decreases (increases) under warm versus cool season warming.

We plotted the 616 HUC-8 basins' SUB_Q and SUB_{ETS} (model-estimated) together with their (seven) basin characteristics and LOWESS-smoothed the results in Figures 6a–6g. To highlight the relationship among SUB_Q, SUB_{ETS} and basin surface characteristics apart from temperature impacts, we parsed the 616 basins into three

zones according to long-term annual mean air temperature (cool: <4°C, moderate: 4–12°C, warm: >12°C). We also plotted scatterplots corresponding to Figures 6a–6g in Figures S9 and S10 in Supporting Information S1, with long-term average annual mean precipitation indicated by colors.

Figures 6a–6c suggest that the increasing SUB_{ETS}, SUB_Q is associated with higher, denser, and deeper vegetation structure in cool zones, while in warm zones the relationship is reversed, and in moderate regions the relationship lies between the two. This is understandable within the VIC model configuration: higher vegetation increases evaporation by increasing roughness length and aerodynamic resistance; denser vegetation increases transpiration by reducing canopy resistance; and deeper root increases transpiration by supporting more water extraction. Therefore, more vegetation enhances the asymmetry of annual evapotranspiration response to seasonal warming, leading to a stronger preference for warm season warming (i.e., more positive SUB_Q and SUB_{ETS} with increasing vegetation) in the cool zones, and contrastingly, a stronger preference for cool season warming (i.e., more negative SUB_Q and SUB_{ETS} with increasing vegetation) in the warm zones.

Figure 6d shows the variation of SUB_{ETS} and SUB_Q with runoff ratio. In cool zones, among basins with runoff ratio <0.5, a higher runoff ratio generally means more rapid spring snowmelt and cooler snowpack, which indicates less sensitive winter snowpack to cool season warming, and more snowmelt occurring in the warm season. This seasonal pattern of snowmelt leads to a stronger preference for evapotranspiration increase under warm season warming (i.e., more positive SUB_Q and SUB_{ETS}). For runoff ratio >0.5, basins with deep snowpacks can experience non-negligible net snowpack decrease on a long-term scale, generating additional streamflow increases. In such basins, the additional streamflow increases more under warm season warming than under cool season warming, which reduces streamflow reduction from warm season warming by a larger degree than from cool season warming, thus reducing SUB_Q. This tendency is stronger in cooler basins with deeper snowpacks and higher runoff ratios, leading to decreasing preference for warm season warming (i.e., decreasing SUB_Q). In warm zones, higher runoff ratios correspond to higher precipitation, mostly in coastal regions (Figures 2d and 2f, S1d in Supporting Information S1) and greater precipitation in winter versus summer (Figure 2e), leading to a stronger preference for cool season warming (i.e., more negative SUB_Q and SUB_{ETS}).

Figure 6e shows relationships among SUB_{ETS}, SUB_Q, and elevation. Across the three temperature zones, there is no significant increasing or decreasing pattern, indicating that elevation's impact on asymmetry mostly comes from its influence on temperature and precipitation (also see Figures S9–S10 in Supporting Information S1), excluding which the remaining impact is insignificant.

The curves in Figures 6f–6g share similar patterns. In cool zones, higher SWE and snow cover fraction favors lower temperature, more water available for evapotranspiration in the warm season, and less sensitive snowmelt (and thus evapotranspiration) to warming in the cool season, thus higher SUB_{ETS}. SUB_Q is smaller than SUB_{ETS} and started to decline for cool zones with SWE >~200 mm and snow cover fraction >~0.6, which is due to net snowpack decrease as discussed above. In moderate zones, SUB_{ETS} and SUB_Q generally increase with higher SWE and snow cover fractions, which relates to lower temperatures. In warm regions, the snow coverage and SWE are both very low, so the snow impact is not substantial (as shown in Figures S9t–u and S10t–u in Supporting Information S1).

The similarity of curve shapes across Figures 6a–6d and 6f–6g can be explained by the spatial coincidence of the above basin characteristics. Regions with more abundant snowpack (higher SWE, snow cover fraction) usually support higher runoff ratio and vegetation growth (Figures S1a–S1d, S1f–S1g in Supporting Information S1). Across Figures 6a–6g, regions with high values of the asymmetry all tend to have lower temperatures. They especially tend toward moderate elevations-high latitude parts of the domain (the northern part of the Columbia River Basin in particular) and moderate latitude-high elevation regions (the northern and eastern parts of the UCRB; Figures 2d and S1h in Supporting Information S1).

Taken over Figures 6a–6g, the SUB_{ETS} generally is lower than the SUB_Q in warm zones and at lower values of the seven basin characteristics for the other two temperature zones, which corresponds with warmer, more arid regions. The SUB_{ETS} generally is higher than the SUB_Q when the values of the seven basin characteristics are higher, corresponding to cooler, more humid basins. The smaller SUB_{ETS} relative to the SUB_Q are due to the compensating effect of warm season evapotranspiration decreases under cool season warming, as discussed in Ban et al. (2020). The larger SUB_{ETS} relative to the SUB_Q generally occur for basins with high snow cover fraction and high SWE, which leads to situations where the net snow storage decline can be non-negligible (Mote

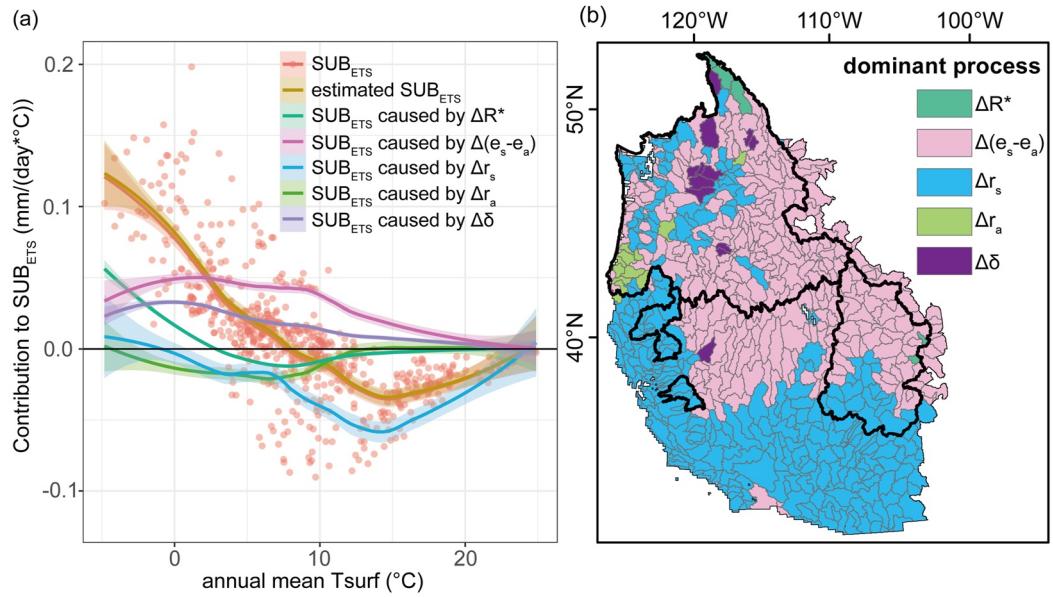

Figure 7. (a) LOWESS-smoothed asymmetry of ET-T sensitivity (SUB_{ETS}, see Equation 6 for definition), estimated SUB_{ETS}, and contribution of the five major ET-related processes to the estimated SUB_{ETS} across values for each of the 616 HUC-8 basins, as a function of annual mean surface temperature; The five processes: Available radiation (R^*), vapor pressure deficit (e_s–e_a), surface resistance (r_s), aerodynamic resistance (r_a), and slope of saturated vapor pressure curve (δ). (b) Dominant processes controlling SUB_{ETS} for each HUC-8 basin. The LOWESS-smoothing span parameter and shading denotation are the same as the ones in Figure 5a.

et al., 2005, 2018), as discussed above. In other words, long-term snow storage decline mitigates the general trend of stronger streamflow responses to warm season warming at cooler regions, at the price of reducing snowpack.

4.5. Processes Dominating Streamflow Response Asymmetry Across Temperatures

Figure 7a shows the five primary ET-T sensitivity-related processes' (see Section 3.5 and Figure 7 captions) contributions to SUB_{ETS} (defined in Equation 6) as a function of annual mean surface temperature. We calculated their contributions to SUB_{ETS} as their contributions to warm season ET-T sensitivity (using derivative expansion, described in Section 3.5) minus those to cool season ET-T sensitivity. We added up the five processes' estimated contributions to SUB_{ETS} (brown curve, Figure 7a), which is quite close to the SUB_{ETS} (red curve, Figure 7a) directly calculated from model output, which confirms the accuracy of the approximation. The process with the largest fractional contribution to SUB_{ETS} is identified as the dominant process on a HUC-8 basin basis (Figure 7b).

Figure 7 suggests that different processes dominate the asymmetry of ET-T sensitivity (SUB_{ETS}) under seasonal warming at different temperatures. The contribution of available radiation change to the ET-T sensitivity asymmetry increases as cooler basins warm (Figure 7a). However, the difference in available radiation changes between warm and cool season warming contributes most to the asymmetry of ET-T sensitivity for only five of the 616 basins, all of which are at the highest latitudes (>50°N) or very high elevations (>3,000 m; Figures 7b and S1e in Supporting Information S1). This result is consistent with the more active snowmelt and albedo-radiation feedback, and therefore enhanced potential evapotranspiration (Neto et al., 2020) in these basins' warm seasons. For basins with moderate temperatures, the difference in vapor pressure deficit change between warm and cool season warming contributes most to the asymmetry of ET-T sensitivity (293 basins), while changes in aerodynamic resistance and slope of saturated vapor pressure curve dominates fewer (12 for both) basins. For basins with the warmest temperatures, sensitivity of ET to warming-induced vapor pressure deficit change starts to decline, while the sensitivity of ET to surface resistance change remains relatively high at high temperatures (see supplement Figure S17 of Ban et al., 2020). Therefore, change in surface resistance becomes the dominant contributor to ET-T sensitivity's asymmetry (294 basins). Over the entire domain, changes in vapor pressure

deficit and surface resistance contribute most to the asymmetry of ET-T sensitivity (587 of the 616 basins) and therefore dominate the annual streamflow response asymmetry.

5. Discussion

Milly and Dunne (2020) and Neto et al. (2020) concluded that increased net radiation from reflective snow loss under warming contributes most to the annual streamflow decline under annual warming for the UCRB. However, in our results, for the asymmetry of streamflow responses to seasonal warming, change in available radiation contributes less than change in vapor pressure deficit and surface resistance across most of the WUS (Figure 7). There are several reasons for this. First, our discussion focuses on the asymmetry of annual streamflow response to seasonal warming instead of the annual streamflow response to annual warming as in Milly and Dunne (2020). Radiation-driven evapotranspiration increase is more evenly split by the warm and cool seasons than are evapotranspiration increases driven by changes in vapor pressure deficit or surface resistance (Figure S12 in Supporting Information S1, taking UCRB as an example). Therefore, changes in vapor pressure deficit and surface resistance contribute more substantially to the seasonal asymmetry of annual streamflow response than do changes in available radiation (Figure S12 in Supporting Information S1). Second, we calculated contributions of vapor pressure deficit change and surface resistance change to evapotranspiration changes explicitly and separately in the Penman–Monteith expansion, while Milly and Dunne (2020) implicitly included contributions from the two processes together in the non-linear term category. Due to the feedback between elevated vapor pressure deficit and elevated surface resistance, if we consider the two factors' total effect on evapotranspiration changes, their contributions partially cancel out, and the remaining net contribution to annual evapotranspiration change under annual 1°C warming is smaller than the contribution from available radiation change in the study area (UCRB) of Milly and Dunne (2020) (Table S2 in Supporting Information S1). Nevertheless, discussing the two factors explicitly and separately is beneficial since the cancellation level varies across different hydroclimate conditions, and varies when discussing the response asymmetry instead of the annual response to annual warming (Figure 7).

We also show in Table S2 in Supporting Information S1 that when contributions from surface resistance change and vapor pressure deficit change partially cancel, the available radiation change still contributes less than the change in the slope of the saturated vapor pressure curve. This contribution ranking differs from Milly and Dunne (2020)'s finding that snow-albedo effect contributes more to streamflow decline than do temperature-associated changes in saturated vapor pressure. This difference in our results and theirs is probably due to differences in the evapotranspiration calculation framework. Our results come from a Penman–Monteith framework that considers the impact of vapor pressure deficit change on actual evapotranspiration, while Milly and Dunne (2020) used a Priestley–Taylor framework that discounts this impact. Under warming, reduced snowpack and albedo elevate net radiation, enhancing latent heat flux and bringing more moisture to the air, which reduces the vapor pressure deficit increment that directly comes from warming. This negative side effect of enhanced radiation on vapor pressure deficit mitigates the radiation-driven evapotranspiration increase under warming somewhat. However, as mentioned above, the vapor pressure deficit impact on evapotranspiration is ignored in Priestley–Taylor framework. As a result, using a Priestley–Taylor framework results in a larger contribution of radiation (e.g., snowmelt-albedo feedback) to evapotranspiration increase and hence streamflow decline under warming.

We recognize that our land surface modeling does not consider the impact of elevated humidity from evapotranspiration increase on vapor pressure deficit, which could overemphasize vapor pressure deficit increase under temperature warming, leading to a larger contribution of vapor pressure deficit change to evapotranspiration increase. To check if this effect is substantial, we compared the relationship between vapor pressure deficit and air temperature in the VIC model and one high-resolution (50 km) general circulation model (CNRM-CM6-1-HR) acquired from the Coupled Model Intercomparison Project (CMIP) version 6 multi-model ensemble (Juckes et al., 2020; Voldoire, 2019). We used the two models' daily historical period from 1950/01/01 to 2014/12/31 for the UCRB (using basin averages) and plotted the results in Figure S13 in Supporting Information S1. Vapor pressure deficit in the coupled model is slightly lower than that in the VIC model at moist pixels, and the two converge in regions with low soil moisture. In general, the difference between the slope of vapor pressure deficit versus air temperature is not substantial between the two models, indicating the feedback between enhanced evapotranspiration and vapor pressure deficit should not substantially affect our findings based on the off-line implementation of the VIC model.

In addition to our model-based evaluation in Section 4.4, we also utilized observation-based estimates (i.e., S_w and S_c in Equation 4) to check their relationships with basin characteristics (Figure S11, detailed discussions see Text S1 in Supporting Information S1). Besides the similarity in a general context, the observation-based results are more inclined to have a stronger streamflow decrease under cool season warming especially in moderate regions, and reflect a stronger suppressive effect of long-term snowpack reduction on streamflow sensitivity to warm season warming in cool regions, compared to results from model-simulations. Supposing the observation-based estimates can represent the reality, these differences may reflect how the real-world sensitivities could deviate from simulations.

Despite these differences, overall similarities between simulated and observation-based results (Figure 4, Figures S4–S7 in Supporting Information S1) suggest that the simulated results are not just reflecting how the model works, but also the streamflow response in the external world. Here, some differences between simulated and observation-based estimates of streamflow response are not unexpected, and we choose to rely on model outputs because: (a) Observation-based estimations treat each year as an individual realization of reference climates, which is less clear and informative than the model simulations treating baseline climatology as the reference climate; (b) Interannual variations in precipitation and their effect on streamflow generally dominate effects of temperature variation, complicating extraction of temperature effects from observations. This is a problem as well in observation-based estimations of elasticity, for example, of annual streamflow to potential evapotranspiration (Xiao et al., 2020); (c) Some other issues in the observation-estimates, including shorter records, linear assumption, fewer predictors, and potential inevitable human disturbances to observations even after screening. There are also limitations in model simulations, such as static and smoothed parameters that may cause stronger spatial-smoothness of asymmetry than in reality.

The streamflow response asymmetry and its controlling mechanisms (characteristics) discussed in this paper represent a refinement of previous runoff-climate studies at much lower spatial resolution (Ban et al., 2020; Das et al., 2011) and for seasonal rather than annual scale of warming (e.g., Milly & Dunne, 2020). Future studies could follow the pathway we've developed to address additional issues such as implications of differential warming for seasonal water scarcity (especially in the dry-season). Exploration of seasonal streamflow responses to differential warming might also explore the implications of vegetation dynamics, and atmosphere-land surface coupling.

6. Conclusions

We examined the complex spatial patterns of annual streamflow relative response to warm versus cool season warming across the WUS. At a much higher granularity (HUC-8), we confirmed relationships between annual streamflow response asymmetry, temperature, and GIW found in our earlier work at much coarser spatial scales (Ban et al., 2020). We also evaluated the observation-based support for model-based sensitivity estimates; examined impacts of different basin surface characteristics on the patterns of annual streamflow relative response to seasonal warming; identified the processes that contribute most to the annual streamflow response asymmetry across the 616 HUC-8 basins, and discussed the relative role of net radiation as drivers to annual streamflow sensitivity to seasonal warming. All of these analyses expand on our previous work (Ban et al., 2020). Additionally, the smooth transition of results from west-to east-of the Continental Divide suggests that our findings could be applied to other similar basins (snow-dominated, asymmetrical seasonal warming).

Based on our work, we conclude that:

1. Using the ratio of annual streamflow decreases resulting from warm versus cool season warming, moist basins with relatively low temperatures, high warm-to-cool-season GIW ratios, and moderate winter snow accumulation have the largest asymmetries (ratio >1). These basins are mostly at high latitude (north of 37.5°N) or high elevation, especially the northern Columbia River basin and most of the Upper Colorado River Basin. Warmer coastal basins have smaller asymmetry (ratio <1). Extremely warm and arid basins (e.g., those bordering on the Mojave and Sonoran Deserts) and extremely cold basins with long snow seasons (e.g., three basins at the northern boundary of the Columbia River Basin) have negative asymmetries, with annual streamflow increases under warm season warming. Extremely arid but moderate temperature basins (e.g., those draining to the Great Basin) also have negative asymmetries, but with annual streamflow increases under cool season

warming. Generally, stronger asymmetry occurs for cooler basins. This is because the ratio between warm and cool season evapotranspiration-temperature sensitivity which constrains the asymmetry is higher for cooler temperatures. Ban et al. (2020) found a similar pattern among four much larger river basins

2. LOWESS-smoothed relationships between basin characteristics and asymmetry of annual streamflow responses from VIC indicate that cool (warm) basins streamflow has an asymmetrical tendency to be more sensitive to warm (cool) season warming. In both types of basins, increased vegetation (height, root depth, and density) enhances the above tendency by enhancing evapotranspiration and thus amplifies ET-T sensitivity. Runoff ratio and snow also enhance the tendency when runoff ratio <0.5, SWE <200 mm, and snow cover fraction <0.6. Above these thresholds, net snowpack decrease causes additional snowmelt, a larger proportion of which occurs under warm season warming than cool season warming, mitigating the tendency of streamflow to decrease under warm season warming. Compared with model-based results, observation-based estimates show less asymmetry toward warm season warming
3. Different warming-associated processes dominate the asymmetry of seasonal evapotranspiration-temperature sensitivity and hence the response asymmetry for annual streamflow across the 616 HUC-8 basins. In the extremely cold basins with the shortest snow-free season with 85% or more of snowmelt-generated streamflow occurring after Apr 1st, available radiation changes that primarily due to reduced snow cover dominate the streamflow response asymmetry; in basins with intermediate temperature, vapor pressure deficit changes dominate, and in basins with the warmest temperatures, surface resistance increases under warmer temperature dominate

Data Availability Statement

Data and codes in this paper are publicly available at the following URLs: GRanD v1.3 database: http://globaldamwatch.org/data/#core_global. USGS GAGESII: https://water.usgs.gov/GIS/metadata/usgswrd/XML/gagesII_Sept2011.xml#stdorder. USGS WaterWatch: https://waterwatch.usgs.gov/index.php?id=wwds_runoff. VIC-4.1.2.g: doi: 10.5281/zenodo.4695040. Other data (and information) used in this paper: doi:10.6084/m9.figshare.14349527.v5. This work was funded in part by a grant from the NOAA Regional Integrated Sciences and Assessments (RISA) program to the California Nevada Climate Applications Program (CNAP) at the Scripps Institution of Oceanography, Grant Nos. NA17OAR4310284, under subaward to the University of California, Los Angeles.

Acknowledgments
We acknowledge Mr. Chandramauli Awasthi and Dr. Sankar Arumugam at North Carolina State University and Dr. Richard Vogel at Tufts University for their help in setting up panel regression with observations in our exploration for the paper. We acknowledge Chen Xin and Lu Su of UCLA Department of Geography for helpful discussions. We acknowledge the World Climate Research Programme, which, through its Working Group on Coupled Modelling, coordinated and promoted CMIP6. We thank the climate modeling groups for producing and making available their model output, which we used in the discussion section, the Earth System Grid Federation (ESGF) for archiving the data and providing access, and the multiple funding agencies who support CMIP6 and ESGF.

References

Adam, J. C., Hamlet, A. F., & Lettenmaier, D. P. (2009). Implications of global climate change for snowmelt hydrology in the twenty-first century. *Hydrological Processes: International Journal*, *23*(7), 962–972. https://doi.org/10.1002/hyp.7201

Ban, Z., Das, T., Cayan, D., Xiao, M., & Lettenmaier, D. P. (2020). Understanding the asymmetry of annual streamflow responses to seasonal warming in the Western US. *Water Resources Research*, e2020WR027158.

Barnett, T. P., Adam, J. C., & Lettenmaier, D. P. (2005). Potential impacts of a warming climate on water availability in snow-dominated regions. *Nature*, *438*(7066), 303–309. https://doi.org/10.1038/nature04141

Barnhart, T. B., Molotch, N. P., Livneh, B., Harpold, A. A., Knowles, J. F., & Schneider, D. (2016). Snowmelt rate dictates streamflow. *Geophysical Research Letters*, *43*(15), 8006–8016. https://doi.org/10.1002/2016gl069690

Bohn, T. J., Livneh, B., Oyler, J. W., Running, S. W., Nijssen, B., & Lettenmaier, D. P. (2013). Global evaluation of MTCLIM and related algorithms for forcing of ecological and hydrological models. *Agricultural and Forest Meteorology*, *176*, 38–49. https://doi.org/10.1016/j.agrformet.2013.03.003

Brakebill, J. W., Wolock, D. M., & Terziotti, S. (2011). Digital hydrologic networks supporting applications related to spatially referenced regression modeling 1. *Journal of the American Water Resources Association*, *47*(5), 916–932. https://doi.org/10.1111/j.1752-1688.2011.00578.x

Condon, L. E., Atchley, A. L., & Maxwell, R. M. (2020). Evapotranspiration depletes groundwater under warming over the contiguous United States. *Nature Communications*, *11*(1), 1–8. https://doi.org/10.1038/s41467-020-14688-0

Das, T., Pierce, D. W., Cayan, D. R., Vano, J. A., & Lettenmaier, D. P. (2011). The importance of warm season warming to western US streamflow changes. *Geophysical Research Letters*, *38*(23). https://doi.org/10.1029/2011gl049660

Dettinger, M. D., Cayan, D. R., Meyer, M. K., & Jeton, A. E. (2004). Simulated hydrologic responses to climate variations and change in the Merced, Carson, and American River basins, Sierra Nevada, California, 1900–2099. *Climatic Change*, *62*(1), 283–317. https://doi.org/10.1023/b:clim.0000013683.13346.4f

Falcone, J. A. (2011). GAGES-II: Geospatial attributes of gages for evaluating streamflow. *US Geological Survey*.

Forbes, W. L., Mao, J., Jin, M., Kao, S.-C., Fu, W., Shi, X., et al. (2018). Contribution of environmental forcings to US runoff changes for the period 1950–2010. *Environmental Research Letters*, *13*(5), 054023. https://doi.org/10.1088/1748-9326/aabb41

Gesch, D. B., Verdin, K. L., & Greenlee, S. K. (1999). New land surface digital elevation model covers the Earth. *Eos, Transactions of American Geophysical Union*, *80*(6), 69–70. https://doi.org/10.1029/99eo00050

Hansen, M. C., DeFries, R. S., Townshend, J. R., & Sohlberg, R. (2000). Global land cover classification at 1 km spatial resolution using a classification tree approach. *International Journal of Remote Sensing*, *21*(6–7), 1331–1364. https://doi.org/10.1080/014311600210209

Hayhoe, K., Cayan, D., Field, C. B., Frumhoff, P. C., Maurer, E. P., Miller, N. L., et al. (2004). Emissions pathways, climate change, and impacts on California. *Proceedings of the National Academy of Sciences*, *101*(34), 12422–12427. https://doi.org/10.1073/pnas.0404500101

Juckes, M., Taylor, K. E., Durack, P. J., Lawrence, B., Mizielinski, M. S., Pamment, A., et al. (2020). The CMIP6 data request (DREQ, version 01.00. 31). *Geoscientific Model Development*, *13*(1), 201–224. https://doi.org/10.5194/gmd-13-201-2020

Lehner, B., Liermann, C. R., Revenga, C., Vörösmarty, C., Fekete, B., Crouzet, P., et al. (2011). High-resolution mapping of the world's reservoirs and dams for sustainable river-flow management. *Frontiers in Ecology and the Environment*, *9*(9), 494–502. https://doi.org/10.1890/100125

Li, D., Wrzesien, M. L., Durand, M., Adam, J., & Lettenmaier, D. P. (2017). How much runoff originates as snow in the western United States, and how will that change in the future? *Geophysical Research Letters*, *44*(12), 6163–6172. https://doi.org/10.1002/2017gl073551

Liang, X., Lettenmaier, D. P., Wood, E. F., & Burges, S. J. (1994). A simple hydrologically based model of land surface water and energy fluxes for general circulation models. *Journal of Geophysical Research: Atmospheres*, *99*(D7), 14415–14428. https://doi.org/10.1029/94jd00483

Livneh, B., Rosenberg, E. A., Lin, C., Nijssen, B., Mishra, V., Andreadis, K. M., et al. (2013). A long-term hydrologically based dataset of land surface fluxes and states for the conterminous United States: Update and extensionsColorado River flow dwindles as warming-driven loss of reflective snow energizes evaporation. *Journal of ClimateScience*, *26367*(236483), 93841252–93921255. https://doi.org/10.1175/jcli-d-12-00508.1

Milly, P. C., & Dunne, K. A. (2020). Colorado River flow dwindles as warming-driven loss of reflective snow energizes evaporation. *Science*, *367*(6483), 1252–1255. https://doi.org/10.1126/science.aay9187

Mote, P. W., Hamlet, A. F., Clark, M. P., & Lettenmaier, D. P. (2005). Declining mountain snowpack in western North America. *Bulletin of the American Meteorological Society*, *86*(1), 39–50. https://doi.org/10.1175/bams-86-1-39

Mote, P. W., Li, S., Lettenmaier, D. P., Xiao, M., & Engel, R. (2018). Dramatic declines in snowpack in the western US. *Npj Climate and Atmospheric Science*, *1*(1), 1–6. https://doi.org/10.1038/s41612-018-0012-1

Neto, A. A. M., Niu, G. Y., Roy, T., Tyler, S., & Troch, P. A. (2020). Interactions between snow cover and evaporation lead to higher sensitivity of streamflow to temperature. *Communications Earth & Environment*, *1*(1), 1–7. https://doi.org/10.1038/s43247-020-00056-9

Qin, Y., Abatzoglou, J. T., Siebert, S., Huning, L. S., AghaKouchak, A., Mankin, J. S., et al. (2020). Agricultural risks from changing snowmelt. *Nature Climate Change*, *10*(5), 459–465. https://doi.org/10.1038/s41558-020-0746-8

Rupp, D. E., Li, S., Mote, P. W., Shell, K. M., Massey, N., Sparrow, S. N., et al. (2017). Seasonal spatial patterns of projected anthropogenic warming in complex terrain: A modeling study of the western US. *Climate Dynamics*, *48*(7–8), 2191–2213. https://doi.org/10.1007/s00382-016-3200-x

Simley, J. D., & Carswell, W. J., Jr. (2009). *The national map—Hydrography: U.S. Geological Survey Fact Sheet, 2009–3054*, p. 4.

Stewart, I. T., Cayan, D. R., & Dettinger, M. D. (2004). Changes in snowmelt runoff timing in western North America under abusiness as usual' climate change scenario. *Climatic Change*, *62*(1), 217–232. https://doi.org/10.1023/b:clim.0000013702.22656.e8

Su, L., Cao, Q., Xiao, M., Mocko, D. M., Barlage, M., Li, D., et al. (2021). Drought variability over the conterminous United States for the past century. *Journal of Hydrometeorology*. https://doi.org/10.1175/jhm-d-20-0158.1

Vano, J. A., & Lettenmaier, D. P. (2014). A sensitivity-based approach to evaluating future changes in Colorado River discharge. *Climatic Change*, *122*(4), 621–634. https://doi.org/10.1007/s10584-013-1023-x

Vano, J. A., Nijssen, B., & Lettenmaier, D. P. (2015). Seasonal hydrologic responses to climate change in the Pacific Northwest. *Water Resources Research*, *51*(4), 1959–1976. https://doi.org/10.1002/2014wr015909

Voldoire, A. (2019). *CNRM-CERFACS CNRM-CERFACS CNRM-CM6-1-HR model output prepared for CMIP6 CMIP historical Earth system grid federation. Version 20200130*. https://doi.org/10.22033/ESGF/CMIP6.4067

Xiao, M., Gao, M., Vogel, R. M., & Lettenmaier, D. P. (2020). Runoff and evapotranspiration elasticities in the western United States: Are they consistent with Dooge's complementary relationship? *Water Resources Research*, *56*(8), e2019WR026719. https://doi.org/10.1029/2019wr026719

Yang, Y., Roderick, M. L., Zhang, S., McVicar, T. R., & Donohue, R. J. (2019). Hydrologic implications of vegetation response to elevated CO_2 in climate projections. *Nature Climate Change*, *9*(1), 44–48. https://doi.org/10.1038/s41558-018-0361-0